Nanoscale

PAPER

View Article Online
View Journal | View Issue

Cite this: *Nanoscale*, 2015, **7**, 4443

Boron nitride nanosheets as barrier enhancing fillers in melt processed composites†

Shaobo Xie,[a] Oana M. Istrate,[a] Peter May,[a] Sebastian Barwich,[a] Alan P. Bell,[b] Umar Khan[a] and Jonathan N. Coleman*[a]

Received 7th December 2014,
Accepted 3rd February 2015

DOI: 10.1039/c4nr07228f

www.rsc.org/nanoscale

In this work we have used melt-processing to mix liquid-exfoliated boron–nitride nanosheets with PET to produce composites for gas barrier applications. Sonication of h-BN powder, followed by centrifugation-based size-selection, was used to prepare suspensions of nanosheets with aspect ratio >1000. The solvent was removed to give a weakly aggregated powder which could easily be mixed into PET, giving a composite containing well-dispersed nanosheets. These composites showed very good barrier performance with oxygen permeability reductions of 42% by adding just 0.017 vol% nanosheets. At low loading levels the composites were almost completely transparent. At higher loading levels, while some haze was introduced, the permeability fell by ~70% on addition of 3 vol% nanosheets.

Introduction

Since the discovery of the exotic properties of graphene,[1] two-dimensional (2D) nanomaterials have attracted renewed interest with this field becoming one of the most active areas of materials science. The study of 2D materials was originally dominated by research into clays[2] and later oxides[3] but now extends beyond graphene[4] to materials such as hexagonal boron nitride (h-BN),[5] transition metal dichalcogenides (TMDs)[6,7] and other more exotic 2D materials such as phosphorene[8] and germanane.[9] The common feature of these 2D materials is that they have strong in-plane covalent bonds within each sheet but interact with each other *via* weak out-of-plane, van der Waals bonds. This generally leads the sheets to stack into 3-dimensional bulk crystals. Today, 2D nanomaterials can be produced by micromechanical cleavage of such layered crystals[10] or bottom-up growth by methods such as chemical vapor deposition.[11] However, these routes are unsuitable for many applications, such as electrodes for electrochemical energy storage and catalysis or as fillers for composites, where large quantities of material are required.[7,12]

For such applications, where considerable masses of material are required, possibly the most appropriate method for producing 2D nanosheets is by liquid phase exfoliation.[13–36] This process involves the sonication[14,15] or shearing[33,36] of layered crystals in certain solvents or surfactant solutions, leading to large amounts of 2D nanosheets which are stabilized against aggregation by interactions with the liquid.[37] This is a general approach and has already been employed to produce mono- or few-layer nanosheets of a number of layered crystals, such as graphene, h-BN, MoS_2, WS_2, MnO_2 and MoO_3. In fact, liquid phase exfoliation is expected to be applicable to any layered materials where the layers are stacked predominately by van der Waals bonds.

Liquid phase exfoliation has a number of advantages in that it is cheap, simple, versatile, and amenable for scale-up.[33,36] It gives suspensions of 2D nanosheets which can be easily processed into thin films, composites, hybrids and a range of other structures. An important feature of liquid phase exfoliation is that it can produce high-quality defect-free 2D nanomaterials in large quantities. Because this process does not induce basal plane defects, the electronic and mechanical properties of the 2D nanosheets are largely preserved. This allows the nanosheets to be used for a range of applications, such as optoelectronics, electrochemistry and eletrocatalysis.[7,32]

Nanosheets produced by liquid phase exfoliation typically have lengths of 100–2000 nm but thicknesses of ~1 nm, resulting in extremely high-aspect-ratio with values beyond 2000 reported.[38] This suggests 2D nanomaterials will become valuable components in polymer composites as reinforcing or conductive fillers or as barrier enhancing agents. For example, monolayer graphene displays the highest thermal conductivity, the highest mechanical stiffness and extraordinary electronic transport properties.[1,39–42] These properties have been harnessed to develop novel graphene-filled composite materials with improved thermal, mechanical and electrical performances.[38,43–45]

[a]*School of Physics, CRANN and AMBER, Trinity College Dublin, Dublin 2, Ireland. E-mail: colemaj@tcd.ie*
[b]*Advanced Microscopy Laboratory (AML), CRANN, Trinity College Dublin, Dublin 2, Ireland*

†Electronic supplementary information (ESI) available. See DOI: 10.1039/c4nr07228f

One of the most important applications of 2D fillers in polymer-based composites are as barrier materials to reduce the permeability of the material to gases. Here, high aspect ratios are particularly important as the 2D filler acts as a physical barrier to diffusing gas molecules: the larger the aspect ratio, the more the gas molecule is slowed down and the bigger the permeability reduction.[46] Due to their low cost, high aspect ratio and low toxicity, nanoclays have been well-studied as barrier-enhancing fillers for polymers. Adding a small fraction of nanoclay has been shown to improve the barrier properties of polymer materials.[2,47,48] Although several commercial polyamide-nanoclay products have been launched, it is still a great challenge to obtain full exfoliation of nanoclay in most other polymer materials when employing conventional processing techniques. This markedly restricts the potential for barrier enhancement of polymers using nanoclays. Even fully exfoliated nanoclays in polyamide have aspect ratios lower than 100.[47] This limits the performance and increases the amount of nanoclay required to achieve a given permeability reduction. For example, it is common for at least 5 wt% nanoclay to be required to reduce the gas permeability by ~40%.[48]

Due to its inherent impermeability to gases, graphene has been utilized as a barrier enhancer in polymer composites.[49,50] Compared to nanoclays, graphene nanosheets tend to have larger aspect ratios, giving them a distinct advantage in areas such as permeability reduction. Hexagonal BN is isostructural with graphene and can be exfoliated in a number of ways,[51,52] including by liquid exfoliation,[12,14,24] to give high aspect ratio nanosheets which are impermeable to gases.[53] Recently, it has been reported that solution processing can be used to mix h-BN with a range of materials, including gelatin, cellulose, chitosan and soy protein,[54–57] resulting in improvements in their barrier properties. In fact, exfoliated h-BN nanosheets (BNNS) are a very attractive additive for barrier composites because their wide bandgap and insulating nature. Because of these properties, it may be possible to decrease the permeability without affecting the optical or electrical properties of the plastic, factors which will be important in certain applications. In addition, the exceptional mechanical properties of h-BN mean that the resultant composites may even have enhanced strength and stiffness compared to the base polymer.[12,58] Importantly for real applications, the achievable production rate for BNNS has been steadily increasing with batches of up to 20 g produced recently.[52]

However, for real applications, it will be important to produce barrier composites by melt, rather than solution, processing. While melt-processable BN-polymer nanocomposites have recently been reported,[59] as far as we know, there is no report describing h-BN as a barrier enhancer in melt processed thermoplastic materials. In the present work, liquid phase exfoliated BN nanosheets have been dispersed into poly(ethylene terephthalate) (PET), a plastic material used in packaging industry, by simple melt-processing. The resultant composites have significantly enhanced oxygen barrier properties compared to PET.

Results and discussion

It is well known that the gas barrier properties of polymer composites filled with 2D materials strongly depend on the volume fraction and the aspect ratio of fillers.[46] In these systems, addition of nanosheets reduces the permeability because the time it takes for gas molecules to diffuse through the film is increased relative to the pure polymer. This is because gas molecules have to follow a "tortuous path", diffusing around the nanosheets.[46] As the degree of tortuosity increases with the nanosheet aspect ratio, it is important to maximise the length while minimising the thickness of the nanosheets used.

In this work we used standard liquid exfoliation procedures[14] (see methods) to produce dispersions of BNNSs in the solvent *N*-methyl-pyrrolidone. We then used a controlled centrifugation protocol[13,60] to remove the small nanosheets in the dispersion leaving us with only larger nanosheets. To assess the dimensions of the exfoliated, size-selected BNNS, transmission electron microscopy, coupled with statistical analysis, was used. Typical images of nanosheets are shown in Fig. 1A–C. These images clearly show few-layer nanosheets with large lateral sizes from hundreds of nanometers to several micrometers, typical of liquid exfoliated BN.[12,58] We measured the length, L, of ~100 nanosheets by statistical analysis of TEM images. The length data is presented as a histogram in Fig. 1D and the mean length of BNNS is ~1.7 μm. Careful inspection of the flake edges[16] allows the estimation of the number of layers per nanosheet, N, as shown in Fig. 1E. The average thickness of BNNS is ~4–5 layers. This is consistent with the thickness of BN nanosheets produced previously by sonication-exfoliation.[12] Then the mean aspect ratio of BNNS can be estimated to be ~1040. This value is in line with our previous data of BNNS[12,58] and slightly below some values reported for liquid exfoliated graphene.[38,60] However, importantly, it is considerably higher than aspect ratios usually reported for clays used in composite applications.[61]

In this work, we opted to produce BN-polymer composites by melting mixing. This is the most common mixing process in the plastics industry and is commonly used to blend different polymer materials or to disperse additives into polymer matrices. Melt mixing is considered a particularly appealing approach to the development of polymer nanocomposites due to its versatility, its compatibility with current polymer processing techniques and its environmentally benign character (no solvents are used). The process involves mixing the molten polymer with fillers under shear. When mixing composite materials, the main challenge is to maximise the dispersion of the filler, ideally resulting in isolated filler particles, surrounded by polymer matrix. We note that for making oxygen-hermetic composites, melt processing is expected to perform better than solution processing. Due to drying or solvent trapping effects, solution processing may induce pores/channels in the resultant composites resulting in a deterioration of the barrier performance.

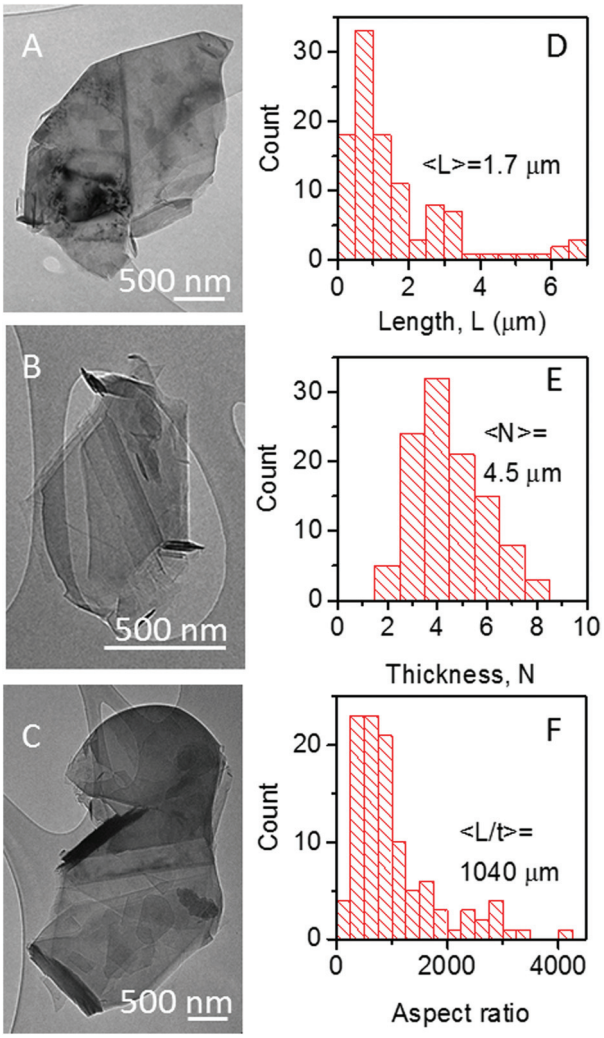

Fig. 1 Exfoliated nanosheets. (A–C) TEM images of exfoliated BN nanosheets. (D–F) Histograms showing (D) nanosheet length, (E) nanosheet thickness and (F) nanosheet aspect ratio. The mean values are given in the panels. In each case, ~100 nanosheets were measured.

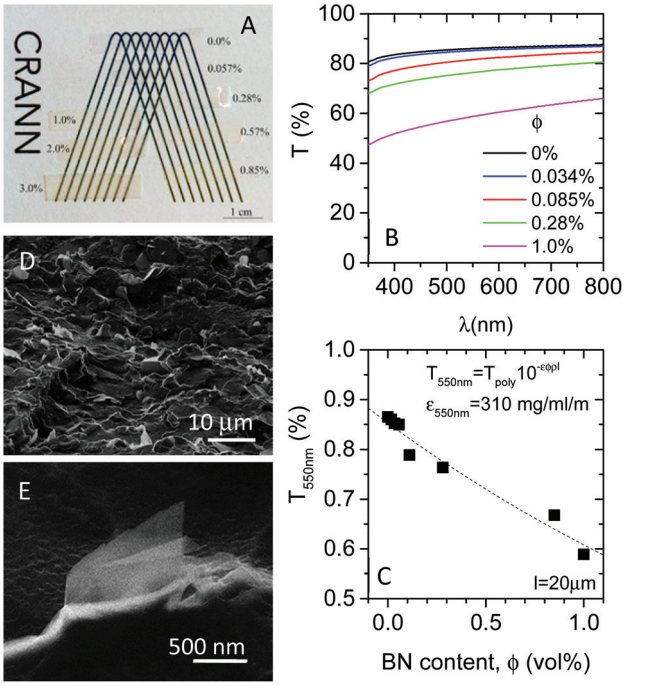

Fig. 2 Composite films. (A) Photograph of composite films with a range of BN volume fractions. (B) Transmission spectra for PET/BN composites of a range of volume fractions (see legend). (C) Transmittance at 550 nm as a function of BN volume fraction. This data is consistent with a BN extinction coefficient of ε_{550nm} = 310 ml mg^{-1} m^{-1}. (D-E) He ion micrographs of fracture surfaces of (D) a 3 vol% and (E) a 0.85 vol% composites.

Previously, we showed that graphene can be dispersed easily into polymer melts when using reaggregated graphene powder as a graphene source.[33,62] Thus, to facilitate composites fabrication by melt mixing, the solvent was removed from the exfoliated BNNSs to give a dry, weakly bound, re-aggregated powder. Such powder are known to be very easy to re-exfoliate in liquids[63,64] and, as mentioned above, can be dispersed in polymer melts under shear reasonably easily.[33,62]

In addition to the materials used, the melt processing conditions are very important for the good dispersion of fillers in polymer matrix. To facilitate the dispersion of BNNS in molten PET, we used a combination of medium and high rotational speeds and appropriate residence time (see details in Methods). Optimum conditions were found during a set of preliminary experiments. The processed compounds were compression moulded into thin films with thickness between 20 and 80 μm. An ice/water bath was used to inhibit crystallization of PET and benefit the formation of transparent films.

Fig. 2A shows the appearance of the PET and PET/BNNS film strips with the indicated volume fractions. They have the same thicknesses of ~20 μm. Visually, all the films are transparent, even at the highest loading of 3.0 vol%, although at the higher BNNS loadings some degree of haze could be seen. However for the very low loading levels, the optical properties were excellent: visually there is very little difference between the composite film with a loading of 0.057 vol% BNNS and the pure PET film. To quantify their optical properties, the films were further characterized using UV-Vis with their transmission spectra shown in Fig. 2B. Shown in Fig. 2C is the transmittance, measured at 550 nm, plotted *versus* the BN volume fraction. While the pure PET exhibits light transmission of 86.5% at 550 nm, the composite film with 0.057 vol% BNNS has transmittance of 85%. The transmittance falls steadily with addition of BN, reaching 60% at a volume fraction of 1.0 vol% BNNS. This can be compared with over 50% loss in light transmittance of polymer film in the presence of only 0.02 vol% graphene sheets.[49] Here, the transmittance falls slowly with BN loading level because the very wide bandgap of BN means that no light is absorbed in the visible region, although some light scattering does occur.[14] This will be a great advantage in plastic packaging industry for applications where transparency is needed. We can quantify the transmittance reduction using the Lambert–Beer law which can be expressed as $T = T_{poly}10^{-\varepsilon Cl}$ where ε is the BN extinction

coefficient [ml mg^{-1} m^{-1}], C is the BN concentration in the matrix [mg ml^{-1}] and l is the film thickness. The concentration is related to the volume fraction by $\phi = C/\rho$ allowing us to write:

$$T = T_{\text{poly}} 10^{-\varepsilon\rho l\phi}$$

This expression fits the data well and is consistent with a BN extinction coefficient of $\varepsilon_{550\ \text{nm}}$ = 310 ml mg^{-1} m^{-1} (using ρ = 2.37 g cm^{-3} as specified by the manufacturer). This is reasonably close to the value of 470 ml mg^{-1} m^{-1} which can be inferred from published data[14] for liquid dispersed BNNSs (550 nm). The difference is probably due to the fact that the scattering cross section of nanosheets is known to be size dependent.[13]

To confirm the dispersion state we analysed the interior of the composites by Helium ion microscopy of the fracture surfaces. Shown in Fig. 2D is an image of a fracture surface of a 3.0 vol% composite. Large number of BNNS can be seen protruding throughout the whole fracture section. Fig. 2E clearly shows few-layer flakes protruding from the polymer. This data implies the dispersion state of BNNSs to be very good in these composites. TEM examination of ultramicrotomed samples (see ESI, Fig. S4†) confirm good dispersion, at least for low volume fractions. Previously, He ion microscopy has revealed extremely good nanosheet alignment in BN-filled polymer composites.[12] Fig. 2D is consistent with the nanosheets being partially aligned. This is supported by X-ray diffraction studies (see ESI, Fig. S5†) which suggest the nanosheets to be somewhat aligned in the plane of the film.

The PET/BNNS composite films are expected to have promising gas barrier properties, due to the good dispersion of BNNS in the PET matrix, the expected impermeability of the BNNSs and their reasonable large aspect ratio. Generally gas transport in polymer films is controlled by both the solubility, S, and the diffusivity, D, of the gas and is described by the permeability, K where $K = SD$. In this work, we measured the oxygen transmission rate (OTR) as a function of time with typical experimental data shown in Fig. 3A for films of PET and three PET/BNNS composites. Initially, the OTR increases sublinearly with time, reflecting nonsteady-state diffusion, before saturating after longer times. The initial portion of the curve is determined by the diffusivity while the steady-state OTR is determined by the permeability. It is clear from this data that the addition of BNNSs has a strong effect on both the non-steady-state and steady-state regions and so both D and K. We calculated the permeability from the steady state portion of the curves using $K = d \times (\text{OTR})_{\text{steady-state}}$, where d is the mean film thickness.

Fig. 3B presents permeability plotted as a function of BN volume fraction. The permeability of the neat PET was 5.72 × 10^{-10} cc cm/(cm^2 s atm) close to accepted literature values of 5.36 × 10^{-10} cc cm/(cm^2 s atm).[65] The permeability falls sharply at very low ϕ and then more gradually at volume fractions above ~0.03 vol%. At our highest loading of BNNS (3 vol%), there is a 70% decrease in the O_2 permeability relative to

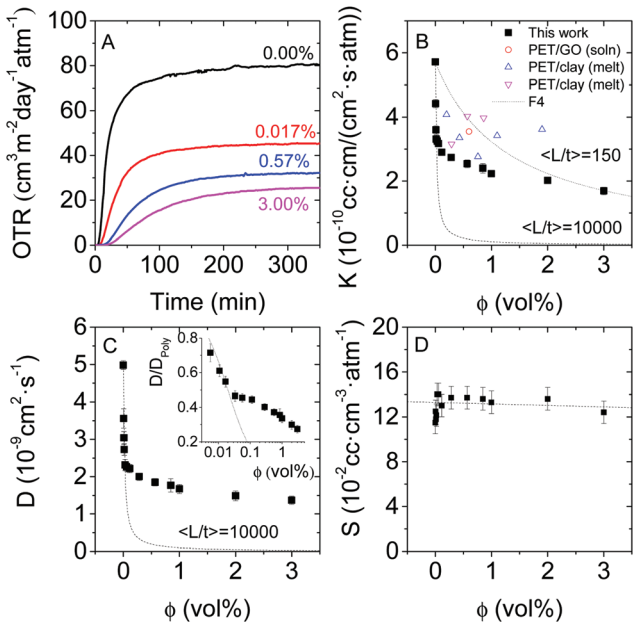

Fig. 3 Barrier properties. (A) Oxygen transmission rate (OTR) plotted as a function of time for films of PET (0%) and three BN/PET composites with volume fractions of up to 3%. (B) Permeability as a function of BN volume fraction. Shown for comparison are data from three papers (PET/GO,[50] PET/clay[67] and PET/oclay,[68] an organic content of 30 wt% was assumed to estimate the organoclay volume fraction in ref. 68). The lines represent theoretical predictions using eqn (1), assuming BN aspect ratios of 10 000 and 100. (C) Diffusivity as a function of BN volume fraction. The lines represent theoretical predictions using eqn (3) assuming BN aspect ratios 10 000. Inset: Composite diffusivity, normalised to that of the polymer, plotted *vs.* ϕ on a semi-log graph. (D) Solubility as a function of BN volume fraction. The dashed line represent the behaviour predicted by the Nielsen model (see text).

the polymer. We note that incorporation of just 0.017 vol% BNNS reduced the permeability by 42% relative to pure PET. Importantly, at this loading level there is a negligible reduction in light transmittance (Fig. 2A).

A number of models have been proposed to describe the dependence of composite permeability on nanosheet aspect ratio and volume fraction.[46] Of these, the simplest is the model of Nielsen[66] which predicts:

$$K = K_{\text{Poly}} \frac{(1-\phi)}{1 + L\phi/2t} \quad (1)$$

where L and t are the mean nanosheet length and thickness respectively. As shown in Fig. 3B the Nielsen model described the initial fall in permeability only if a BNNS aspect ratio of L/t = 10 000 is assumed. This is considerably higher than the measured value of L/t = 1040 and is certainly unrealistic. The origin of this discrepancy is not currently understood. The data begins to deviate from the theoretical line for $\phi \sim 0.03$ vol%. The permeability at the highest volume fractions around 2–3 vol% are consistent with a BNNs aspect ratio of L/t = 150. This suggests that the slow saturation of permeability for volume fractions above ~0.03 vol% is associated with BNNS aggregation. In fact mechanical measurements (see ESI, Fig. S3†) show

the composite stiffness to increase with volume fraction up to $\phi \sim 0.02$, after which the modulus falls. Such a fall off usually denotes aggregation effects. For example, previous mechanical measurements on solution processed BNNS/polymer composites were consistent with an aggregation threshold of 0.15 vol%.[12]

We can compare this data to that reported for other nanocomposites produced by melt processing (data also shown in Fig. 3B).[67,68] Very recently, Wang *et al.* used aqueous clay slurry mixing with molten PET to make PET/clay composites, observing 29% and 52% decreases in oxygen permeability at the clay loading of 0.5 wt% and 2 wt%, respectively.[67] However higher loadings of clay did not result in further reductions due to nanosheet aggregation. Frounchi *et al.* used a Nanolin organoclay to make PET/clay composites by melt processing and obtained ~45% decrease in oxygen permeability with 1 wt% clay content.[68] Similarly, further addition of organoclay in PET did not improve the oxygen barrier properties. Recent work[50] indicated that 38% decrease in oxygen permeability coefficient of PET can be obtained with 1 wt% graphene sheets by solution processing. As shown in Fig. 3B, the BN/PET data obtained here surpasses all of these results. However, we note that much larger improvements may be possible. Al-Jabareen *et al.* reported PET composites filled with graphite nanoplatelets (GNP) which showed oxygen transmission rates which were reduced by 99% relative to the host polymer using only 1.5 wt% GNP.[69] However, as the permeabilities were not reported, this work has not been included in Fig. 3B. In addition, we note that large permeability reductions can be achieved, not by mixing the nanosheets into the polymer, but by coating the nanosheets onto the polymer surface using layer by layer assembly methods.[70,71]

We also calculated the diffusivity *via* a "half-time" method, which is a modification of the conventional time-lag technique and suitable for the measurement at atmospheric pressure.[72] Under these circumstances, the diffusion coefficient is given by:

$$D = \frac{d^2}{7.2t_{1/2}} \quad (2)$$

where d is the film thickness (here expressed in cm) and $t_{1/2}$ (in seconds) is the half of the time required to reach equilibrium OTR. Fig. 3C shows the dependence of diffusion coefficient on the volume fraction of BN. It is very similar to that of permeability curve (Fig. 3B) indicating that the permeability reduction is indeed due to the introduction of tortuosity. In Nielsen's model, the diffusion coefficient is given by[46]

$$D = \frac{D_{\mathrm{Poly}}}{1 + L\phi/2t} \quad (3)$$

Indeed this expression matches well with the sharp drop in D as long as L/t = 10 000 is used, consistent with the permeability data. In order to more clearly see the effect of the nanosheets on the diffusivity at low loading, we plot D/D_{Poly} *vs.* ϕ on a semi-log plot in the inset of Fig. 3C. This plot clearly shows a steep reduction in diffusivity at very low nanosheet loading levels, although the fall-off slows for volume fractions above 0.035%. This behaviour is interesting as it emphasises how effective high aspect ratio nanosheets can be at slowing gas transport even at very low loading levels.

By combining the data for permeability with that of diffusion coefficient, we can calculate the solubility. This is roughly constant at ~0.1 cc cm^{-3} atm^{-1} as plotted *versus* BN volume fraction in Fig. 3D. The Nielsen model predicts the gas solubility to vary very weakly with filler loading level: $S = S_{\mathrm{Poly}}(1 - \phi)$.[46] Indeed this expression is consistent with our data within error as shown in Fig. 3D. It should be noted that, in addition to our permeability data, our diffusivity and solubility data for pristine PET are also consistent with the literature.[65]

In addition, to improving the barrier properties, the presence of BNNS brings additional advantages. For example, addition of BNNS improves the thermal (Fig. S1†), thermal-oxidative stability (Fig. S2†) and mechanical (Fig. S3†) properties of its PET composites. We believe this combination of advantages will be useful in a number of applications.

Conclusions

In summary, liquid phase exfoliation, coupled with centrifugation-based size selection was used to produce BNNS with aspect ratios of >1000. The solvent was removed and the resultant reaggregated powder melt-mixed with PET to produce composites films. Microscopy showed the nanosheets to be well-dispersed in the matrix. The films were transparent and of good optical quality, showing only very slight haze at low BN content. We found the oxygen permeability to fall rapidly at low BN content but more slowly once the volume fraction passed ~0.2 vol%. A permeability reduction of 70% was observed for a BNNS loading level of 3 vol%.

This data shows the permeability reduction to be associated with suppression of diffusion, rather than the reduction of solubility of O_2. The diffusion coefficient is reduced due to the introduction of tortuous paths on the addition of BNNSs to the matrix.

We believe BNNS are potentially useful fillers for barrier composites. Their impermeability, coupled with their potentially high aspect ratios, makes them ideal for this application. In addition, their large bandgap means that they do not contribute to absorption of light while their insulating nature means they will not affect the electrical properties of the polymer. We believe the permeability of PET/BN composites can be further reduced by using BNNS with higher aspect ratio or by using post-stretching leading to better alignment of BNNS in composites.[58]

Methods

Experimental procedure

Three grams of as-supplied boron nitride powder (H.C. Starck GmbH h-BN, Grade A 01) was added to 60 ml of *N*-methylpyrrolidone (NMP) in a 80 ml capacity, flat bottomed metal

beaker. This mixture was sonicated for 48 h using a flat head probe sonic tip (Hielscher UP200S). The beaker was connected to a chiller for cooling the system during sonication. The resultant dispersion was centrifuged (Thermo scientific, Model: Heraeus Megafuge 16 Centrifuge, Rotor: TX-400 Swinging Bucket Rotor with auto lock system) at 700 rpm for 45 min. This results in the separation of small nanosheets (supernatant) from larger nanosheets and unexfoliated crystallites (sediment). The supernatant was decanted and the sediment was re-dispersed in fresh NMP by bath sonication for 1 h. This re-dispersed sediment was then centrifuged at 300 rpm for 20 min to remove any unexfoliated crystallites. This results in a supernatant which contains the desired large nanosheets. The collected supernatant was filtered through polyester membranes (pore size 0.4 μm). The filtered material was washed with isopropanol (IPA) and dried overnight in an oven at 60 °C under vacuum. The size-selected, dried BN powders were re-dispersed in IPA by mild bath sonication (Branson 1510E-MT sonic bath) to give a stock dispersion at concentrations of 2 mg ml^{-1}. To assess the exfoliation state of the dispersed BNNS and to measure their dimensions, a few drops of this dispersion were dropped onto holey carbon grids (400 mesh) and analysed using a JEOL 2100 TEM at 200 kV.

A food-grade poly(ethylene terephthalate) resin, commercially known as CLEARTUF P82 (intrinsic viscosity = 0.80 ± 0.02) was obtained from Plastipak Italia Preforme SRL. PET and PET/BNNS composites with a load varying from 0.017 vol% to 3.0 vol% were melt compounded on a Brabender internal mixer at 251 °C. The melt mixing was performed at first by adding a part of PET pellets to the mixing bowl. The torque increased to a very high value when the polymer started to melt. Once the torque started to diminish, finely ground BNNS powder was gradually added into the mixing bowl. When the torque started to decrease again from the high value, the remaining PET pellets was added to the mixer. Generally all the materials were loaded into the mixer within 2 min. The mixing was performed at an initial speed of 50 rpm for 4 min; then the rotor speed was raised to 100 rpm within 1 min and the compounding was conducted at this speed for another 5 min. The overall batch weight was kept constant at 40 g. PET and PET/BNNS films were prepared by compression molding in a hot press at 280 °C with a pressure of 40 kN. A DupontTM Kapton® polyimide film was placed between two plates of the hot press to prevent adhesion. After pressing, the samples were immediately quenched into ice water. All PET raw materials and the prepared compounds were dried at 120 °C overnight under vacuum prior to melt processing.

Equipment

Optical transmission spectra were recorded using a Cary Varian 6000i. Helium ion microscopy was performed on film fracture surfaces with a Zeiss Orion Plus. All images were acquired using an accelerating voltage of 30 kV and a beam current of 0.5–1 pA. Secondary electrons produced by incident helium ions are detected using an Everhart–Thornley detector. This image signal was averaged over 32 or 64 line scans. Charge compensation was achieved using an electron flood gun.

Oxygen transmission rates (OTR) of pristine PET and PET/BNNS composites films were measured using a Systech Illinois instruments Model 8001 oxygen permeation analyser, which employs the continuous-flow cell method approved by ASTM D 3985–05. Ultra high purity nitrogen was used as the carrier gas at flow rate of 10 ml min^{-1} and pure oxygen was used as the test gas at a rate of 20 ml min^{-1}. The test area was 5 cm^2 using an aluminium mask. The test conditions were 23 °C, 0% relative humidity and 1 atm pressure. The instrument was calibrated at 23 °C with NIST approved 23 μm standard PET film of known OTR values. Prior to the test, the films were conditioned in nitrogen inside the cell for at least 24 h to remove traces of atmospheric oxygen. The conditioning was continued until a steady baseline was obtained where the oxygen flux changed by less than 1% for a 30 min cycle. The permeability (P) was calculated by multiplying the measured steady state transmission rate by the average sample thickness. The solubility coefficient (S) was calculated using the equation: $S = P/D$. At least two separate films were measured for each sample and the averaged value was reported.

Acknowledgements

We thank SAB Miller for funding this research project. We also acknowledge funding from the European Union Seventh Framework Programme under grant agreement no 604391 Graphene Flagship. We have also received support from the Science Foundation Ireland (SFI) funded centre AMBER (SFI/12/RC/2278). In addition, JNC acknowledges the European Research Council (SEMANTICS). We also thank the Advanced Microscopy Lab for help with microscopic analysis.

References

1 K. S. Novoselov, A. K. Geim, S. V. Morozov, D. Jiang, Y. Zhang, S. V. Dubonos, I. V. Grigorieva and A. A. Firsov, *Science*, 2004, **306**, 666–669.
2 E. P. Giannelis, *Adv. Mater.*, 1996, **8**, 29–35.
3 M. Osada and T. Sasaki, *J. Mater. Chem.*, 2009, **19**, 2503–2511.
4 K. S. Novoselov, V. I. Fal'ko, L. Colombo, P. R. Gellert, M. G. Schwab and K. Kim, *Nature*, 2012, **490**, 192–200.
5 Y. Lin and J. W. Connell, *Nanoscale*, 2012, **4**, 6908–6939.
6 Q. H. Wang, K. Kalantar-Zadeh, A. Kis, J. N. Coleman and M. S. Strano, *Nat. Nanotechnol.*, 2012, **7**, 699–712.
7 M. Chhowalla, H. S. Shin, G. Eda, L. J. Li, K. P. Loh and H. Zhang, *Nat. Chem.*, 2013, **5**, 263–275.
8 E. S. Reich, *Nature*, 2014, **506**, 19–19.
9 E. Bianco, S. Butler, S. Jiang, O. D. Restrepo, W. Windl and J. E. Goldberger, *ACS Nano*, 2013, **7**, 4414–4421.

10 K. S. Novoselov, D. Jiang, F. Schedin, T. J. Booth, V. V. Khotkevich, S. V. Morozov and A. K. Geim, *Proc. Natl. Acad. Sci. U. S. A.*, 2005, **102**, 10451–10453.
11 L. Song, L. J. Ci, H. Lu, P. B. Sorokin, C. H. Jin, J. Ni, A. G. Kvashnin, D. G. Kvashnin, J. Lou, B. I. Yakobson and P. M. Ajayan, *Nano Lett.*, 2010, **10**, 3209–3215.
12 U. Khan, P. May, A. O'Neill, A. P. Bell, E. Boussac, A. Martin, J. Semple and J. N. Coleman, *Nanoscale*, 2013, **5**, 581–587.
13 C. Backes, R. J. Smith, N. McEvoy, N. C. Berner, D. McCloskey, H. C. Nerl, A. O'Neill, P. J. King, T. Higgins, D. Hanlon, N. Scheuschner, J. Maultzsch, L. Houben, G. S. Duesberg, J. F. Donegan, V. Nicolosi and J. N. Coleman, *Nat. Commun.*, 2014, **5**, 4576.
14 J. N. Coleman, M. Lotya, A. O'Neill, S. D. Bergin, P. J. King, U. Khan, K. Young, A. Gaucher, S. De, R. J. Smith, I. V. Shvets, S. K. Arora, G. Stanton, H. Y. Kim, K. Lee, G. T. Kim, G. S. Duesberg, T. Hallam, J. J. Boland, J. J. Wang, J. F. Donegan, J. C. Grunlan, G. Moriarty, A. Shmeliov, R. J. Nicholls, J. M. Perkins, E. M. Grieveson, K. Theuwissen, D. W. McComb, P. D. Nellist and V. Nicolosi, *Science*, 2011, **331**, 568–571.
15 Y. Hernandez, V. Nicolosi, M. Lotya, F. M. Blighe, Z. Y. Sun, S. De, I. T. McGovern, B. Holland, M. Byrne, Y. K. Gun'ko, J. J. Boland, P. Niraj, G. Duesberg, S. Krishnamurthy, R. Goodhue, J. Hutchison, V. Scardaci, A. C. Ferrari and J. N. Coleman, *Nat. Nanotechnol.*, 2008, **3**, 563–568.
16 U. Khan, A. O'Neill, M. Lotya, S. De and J. N. Coleman, *Small*, 2010, **6**, 864–871.
17 M. Lotya, Y. Hernandez, P. J. King, R. J. Smith, V. Nicolosi, L. S. Karlsson, F. M. Blighe, S. De, Z. M. Wang, I. T. McGovern, G. S. Duesberg and J. N. Coleman, *J. Am. Chem. Soc.*, 2009, **131**, 3611–3620.
18 M. Lotya, P. J. King, U. Khan, S. De and J. N. Coleman, *ACS Nano*, 2010, **4**, 3155–3162.
19 A. O'Neill, U. Khan and J. N. Coleman, *Chem. Mater.*, 2012, **24**, 2414–2421.
20 G. Cunningham, M. Lotya, C. S. Cucinotta, S. Sanvito, S. D. Bergin, R. Menzel, M. S. P. Shaffer and J. N. Coleman, *ACS Nano*, 2012, **6**, 3468–3480.
21 L. Zhang, Z. J. Zhang, C. Z. He, L. M. Dai, J. Liu and L. X. Wang, *ACS Nano*, 2014, **8**, 6663–6670.
22 K. G. Zhou, N. N. Mao, H. X. Wang, Y. Peng and H. L. Zhang, *Angew. Chem., Int. Ed.*, 2011, **50**, 10839–10842.
23 A. B. Bourlinos, V. Georgakilas, R. Zboril, T. A. Steriotis and A. K. Stubos, *Small*, 2009, **5**, 1841–1845.
24 C. Y. Zhi, Y. Bando, C. C. Tang, H. Kuwahara and D. Golberg, *Adv. Mater.*, 2009, **21**, 2889–2893.
25 F. Torrisi, T. Hasan, W. Wu, Z. Sun, A. Lombardo, T. S. Kulmala, G.-W. Hsieh, S. Jung, F. Bonaccorso, P. J. Paul, D. Chu and A. C. Ferrari, *ACS Nano*, 2012, **6**, 2992–3006.
26 A. Ciesielski and P. Samori, *Chem. Soc. Rev.*, 2014, **43**, 381–398.
27 X. Cui, C. Zhang, R. Hao and Y. Hou, *Nanoscale*, 2011, **3**, 2118–2126.
28 L. Guardia, M. J. Fernandez-Merino, J. I. Paredes, P. Solis-Fernandez, S. Villar-Rodil, A. Martinez-Alonso and J. M. D. Tascon, *Carbon*, 2011, **49**, 1653–1662.
29 D. Nuvoli, L. Valentini, V. Alzari, S. Scognamillo, S. B. Bon, M. Piccinini, J. Illescas and A. Mariani, *J. Mater. Chem.*, 2011, **21**, 3428–3431.
30 M. Zhang, R. R. Parajuli, D. Mastrogiovanni, B. Dai, P. Lo, W. Cheung, R. Brukh, P. L. Chiu, T. Zhou, Z. Liu, E. Garfunkel and H. He, *Small*, 2010, **6**, 1100–1107.
31 D. Hanlon, C. Backes, T. M. Higgins, M. Hughes, A. O'Neill, P. King, N. McEvoy, G. S. Duesberg, B. M. Sanchez, H. Pettersson, V. Nicolosi and J. N. Coleman, *Chem. Mater.*, 2014, **26**, 1751–1763.
32 V. Nicolosi, M. Chhowalla, M. G. Kanatzidis, M. S. Strano and J. N. Coleman, *Science*, 2013, **340**, 1226419.
33 K. R. Paton, E. Varrla, C. Backes, R. J. Smith, U. Khan, A. O'Neill, C. Boland, M. Lotya, O. M. Istrate, P. King, T. Higgins, S. Barwich, P. May, P. Puczkarski, I. Ahmed, M. Moebius, H. Pettersson, E. Long, J. Coelho, S. E. O'Brien, E. K. McGuire, B. M. Sanchez, G. S. Duesberg, N. McEvoy, T. J. Pennycook, C. Downing, A. Crossley, V. Nicolosi and J. N. Coleman, *Nat. Mater.*, 2014, **13**, 624–630.
34 J. N. Coleman, *Acc. Chem. Res.*, 2013, **46**, 14–22.
35 R. J. Smith, P. J. King, M. Lotya, C. Wirtz, U. Khan, S. De, A. O'Neill, G. S. Duesberg, J. C. Grunlan, G. Moriarty, J. Chen, J. Z. Wang, A. I. Minett, V. Nicolosi and J. N. Coleman, *Adv. Mater.*, 2011, **23**, 3944–3948.
36 E. Varrla, K. R. Paton, C. Backes, A. Harvey, R. J. Smith, J. McCauley and J. N. Coleman, *Nanoscale*, 2014, **6**, 11810–11819.
37 J. M. Hughes, D. Aherne and J. N. Coleman, *J. Appl. Polym. Sci.*, 2013, **127**, 4483–4491.
38 P. May, U. Khan, A. O'Neill and J. N. Coleman, *J. Mater. Chem.*, 2012, **22**, 1278–1282.
39 A. A. Balandin, S. Ghosh, W. Z. Bao, I. Calizo, D. Teweldebrhan, F. Miao and C. N. Lau, *Nano Lett.*, 2008, **8**, 902–907.
40 C. Lee, X. D. Wei, J. W. Kysar and J. Hone, *Science*, 2008, **321**, 385–388.
41 Y. B. Zhang, Y. W. Tan, H. L. Stormer and P. Kim, *Nature*, 2005, **438**, 201–204.
42 K. S. Novoselov, A. K. Geim, S. V. Morozov, D. Jiang, M. I. Katsnelson, I. V. Grigorieva, S. V. Dubonos and A. A. Firsov, *Nature*, 2005, **438**, 197–200.
43 K. M. F. Shahil and A. A. Balandin, *Nano Lett.*, 2012, **12**, 861–867.
44 U. Khan, P. May, A. O'Neill and J. N. Coleman, *Carbon*, 2010, **48**, 4035–4041.
45 C. S. Boland, U. Khan, C. Backes, A. O'Neill, J. McCauley, S. Duane, R. Shanker, Y. Liu, I. Jurewicz, A. B. Dalton and J. N. Coleman, *ACS Nano*, 2014, **8**, 8819–8830.
46 G. Choudalakis and A. D. Gotsis, *Eur. Polym. J.*, 2009, **45**, 967–984.
47 E. Picard, A. Vermogen, J. F. Gerard and E. Espuche, *J. Membr. Sci.*, 2007, **292**, 133–144.

48 S. S. Ray, *Macromol. Chem. Phys.*, 2014, **215**, 1162–1179.
49 O. C. Compton, S. Kim, C. Pierre, J. M. Torkelson and S. T. Nguyen, *Adv. Mater.*, 2010, **22**, 4759–4763.
50 S. H. Shim, K. T. Kim, J. U. Lee and W. H. Jo, *ACS Appl. Mater. Interfaces*, 2012, **4**, 4184–4191.
51 X. Wang, C. Zhi, L. Li, H. Zeng, C. Li, M. Mitome, D. Golberg and Y. Bando, *Adv. Mater.*, 2011, **23**, 4072–4076.
52 X.-B. Wang, Q. Weng, X. Wang, X. Li, J. Zhang, F. Liu, X.-F. Jiang, H. Guo, N. Xu, D. Golberg and Y. Bando, *ACS Nano*, 2014, **8**, 9081–9088.
53 A. Itakura, M. Tosa, S. Ikeda and K. Yoshihara, *Vacuum*, 1996, **47**, 697–700.
54 S. K. Kisku and S. K. Swain, *J. Am. Ceram. Soc.*, 2012, **95**, 2753–2757.
55 S. K. Swain, S. Dash, C. Behera, S. K. Kisku and L. Behera, *Carbohydr. Polym.*, 2013, **95**, 728–732.
56 S. Dash and S. K. Swain, *Compos. Sci. Technol.*, 2013, **84**, 39–43.
57 J. Biscarat, M. Bechelany, C. Pochat-Bohatier and P. Miele, *Nanoscale*, 2015, **7**, 613–618.
58 R. Jan, P. May, A. P. Bell, A. Habib, U. Khan and J. N. Coleman, *Nanoscale*, 2014, **6**, 4889–4895.
59 X. Huang, S. Wang, M. Zhu, K. Yang, P. Jiang, Y. Bando, D. Golberg and C. Zhi, *Nanotechnology*, 2015, **26**, 015705.
60 U. Khan, A. O'Neill, H. Porwal, P. May, K. Nawaz and J. N. Coleman, *Carbon*, 2012, **50**, 470–475.
61 S. Pavlidou and C. D. Papaspyrides, *Prog. Polym. Sci.*, 2008, **33**, 1119–1198.
62 O. M. Istrate, K. R. Paton, U. Khan, A. O'Neill, A. P. Bell and J. N. Coleman, *Carbon*, 2014, **78**, 243–249.
63 S. Barwich, U. Khan and J. N. Coleman, *J. Phys. Chem. C*, 2013, **117**, 19212–19218.
64 U. Khan, H. Porwal, A. O'Neill, K. Nawaz, P. May and J. N. Coleman, *Langmuir*, 2011, **27**, 9077–9082.
65 A. Hiltner, R. Y. F. Liu, Y. S. Hu and E. Baer, *J. Polym. Sci., Part B: Polym. Phys.*, 2005, **43**, 1047–1063.
66 L. E. Nielsen, *J. Macromol. Sci., Part A: Pure Appl. Chem.*, 1967, **1**, 929–942.
67 Y. Wang and S. A. Jabarin, *J. Appl. Polym. Sci.*, 2013, **129**, 1455–1465.
68 M. Frounchi and A. Dourbash, *Macromol. Mater. Eng.*, 2009, **294**, 68–74.
69 A. Al-Jabareen, H. Al-Bustami, H. Harel and G. Marom, *J. Appl. Polym. Sci.*, 2013, **128**, 1534–1539.
70 B. Stevens, E. Dessiatova, D. A. Hagen, A. D. Todd, C. W. Bielawski and J. C. Grunlan, *ACS Appl. Mater. Interfaces*, 2014, **6**, 9942–9945.
71 F. Xiang, P. Tzeng, J. S. Sawyer, O. Regev and J. C. Grunlan, *ACS Appl. Mater. Interfaces*, 2014, **6**, 6040–6048.
72 K. D. Ziegel, H. k. Frensdor and D. E. Blair, *J. Polym. Sci., Part A-2*, 1969, **7**, 809–819.